THE JOURNAL OF
PHYSICAL
CHEMISTRY C
LETTERS

2007, *111,* 9001−9004
Published on Web 06/02/2007

Structural Surface Investigations of Cerium−Zirconium Mixed Oxide Nanocrystals with Enhanced Reducibility

**Juan C. Hernández,[†] Ana B. Hungría,[‡] José A. Pérez-Omil,*[,†,§] Susana Trasobares,[†]
Serafín Bernal,[†] Paul A. Midgley,[‡] Ali Alavi,[§] and José J. Calvino[†]**

Departamento de Ciencia de los Materiales e Ingeniería Metalúrgica y Química Inorgánica, Universidad de Cádiz, 11510 Puerto Real, Spain, Department of Materials Science and Metallurgy, University of Cambridge, Cambridge CB2 3QZ, UK, and Department of Chemistry, University of Cambridge, Cambridge CB2 1EW, UK

Received: March 29, 2007; In Final Form: May 3, 2007

High-resolution electron microscopy, high-angle annular dark field images, electron tomography data, and density functional theory calculations are presented that show the occurrence of significant structural and surface modifications in a nanocrystalline sample of cerium−zirconium mixed oxide upon high-temperature reduction with hydrogen followed by mild oxidation. Our findings may lend further support to a recently proposed model in accordance with which the enhanced reducibility exhibited by the mixed oxide after this treatment is due to parallel modifications occurred in its surface chemistry.

Introduction

The incorporation of ceria−zirconia mixed oxides to three-way catalysts has represented a major breakthrough point in automotive aftertreatment technology.[1,2] After that, a continuous growing interest in their catalytic application in other fields has been seen.[3−5] The oxygen exchange capability of the Ce−Zr mixed oxides is a key feature lying behind most of their catalytic applications. As such, numerous studies have been devoted to better understanding their very challenging redox properties.[6−16] It is well established that heating these materials in hydrogen at high temperature (Tredn $>$ 1173 K) followed by a mild reoxidation treatment (Treoxn $=$ 873 K) (i.e. a severe reduction $+$ mild oxidation (SR-MO)) leads to oxide samples with enhanced reducibility.[9−16]

As shown in some recent electron microscopy studies,[16−19] the SR-MO treatment induces the occurrence of a disorder−order transition in the cationic sublattice of the ceria−zirconia mixed oxides. As a result, an ordered arrangement of Ce^{4+} and Zr^{4+} cations, like the one exhibited by pyrochlore-related structures, is observed.[20,21] On the other hand, it has been reported also very recently that the improvement in the low-temperature reducibility induced after a SR-MO cycle is closely related to the capability of the resulting oxide surfaces for activating the hydrogen molecule dissociation.[16] Previous methanol adsorption studies point to surface cation rearrangement after the redox cycles.[10,12] For these reasons there is a major interest to investigate at atomic level the influence of the cationic sublattice disorder−order transformation on the surface structure of these mixed oxides. This work reports some recent findings related to this topic using high-resolution electron microscopy (HREM), high-angle annular dark field−scanning transmission electron microscopy (HAADF-STEM), and electron tomography techniques. Likewise, to arrive at a finer interpretation of the experimental data, density functional theory (DFT) and computer imaging calculations have also been used.

Experimental Methods

The fresh, low surface area, $Ce_{0.62}Zr_{0.38}O_2$ sample investigated in this paper has been kindly provided by Grace Davison. The SR-MO cycle consists in two steps: first step (SR), was reduction under flowing H_2 at 1223 K for 5 h followed by evacuation in a flow of He at the same temperature for 1 h; and second step (MO), after cooling in He the sample was reoxidized, first at 298 K with O_2 pulses until no further consumption was observed, and later on by heating under flowing O_2 (5%)/He at 773 K for 1 h. The BET surface area of the fresh and SR-MO-treated samples were 19 $m^2\ g^{-1}$ and 16 $m^2\ g^{-1}$, respectively.

HREM and HAADF images were recorded on a JEOL 2010-FEG TEM/STEM electron microscope equipped with a JEOL HAADF detector. The HREM and HAADF images simulations were performed using the EMS[22] and Kirkland's[23] programs, respectively. The structural supercells needed for simulation were built using Rhodius software[24] from the University of Cádiz.

HAADF STEM tomography was performed on a 200 kV FEI Tecnai F20 TEM/STEM electron microscope. Image alignment and reconstructions were performed using the FEI software Inspect 3D and visualized using Amira.[25]

Results and Discussion

Figure 1 shows HREM images of a $Ce_{0.62}Zr_{0.38}O_2$ sample before (a) and after (b) the SR-MO treatment. The structure of

---

* To whom correspondence should be addressed. E-mail: jose.perez-omil@uca.es. Tel: +34-956016333. Fax: +34-956016288.
[†] Universidad de Cádiz.
[‡] Department of Materials Science and Metallurgy, University of Cambridge.
[§] Department of Chemistry, University of Cambridge.

10.1021/jp072466a CCC: $37.00

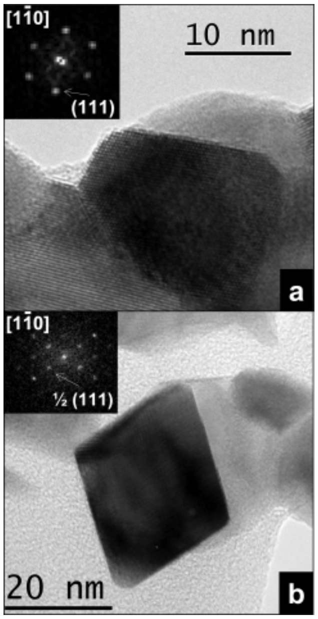

Figure 1. Representative HREM images for the fresh (a) and SR-MO-treated (b) Ce/Zr mixed oxides. Insets show FT of the nanocrystal lattices.

the fresh sample corresponds to that of a solid solution with a fluorite type structure and a random distribution of Ce and Zr in the cationic sublattice. Fourier transforms (FTs) obtained from these images, such as the one in the inset in Figure 1a, show spots corresponding to only the cubic or tetragonal polymorphs of the mixed oxide. In contrast, after SR-MO, the presence of 1/2 {111} superstructure spots, characteristic of a pyrochlore-related phase, are clearly identified.[17,21]

The structure of a fully oxidized pyrochlore-related cerium−zirconium mixed oxide has been modeled using Car−Parrinello molecular dynamics,[26] as implemented in the CPMD code.[27] The electronic structure has been described in the framework of the DFT within the local density aproximation. The valence electrons wavefunctions are expanded in a plane wave basis set with an energy cutoff fixed to 60 Hartrees, and the core-valence interactions were accounted through norm-conserving pseudopotentials. A 2 × 2 × 2 fluorite-like superstructure with a pyrochlore-like Ce/Zr sublattice ordering was used as starting structure. Several molecular dynamics calculations were applied reducing the initial temperature (300 K) and scaling the ionic velocities to find the minimum energy situation. The final relaxed model was achieved when the energy of the system was decreased 79.7 kJ mol^{-1} of oxidized pyrochlore. Wavefunction and geometry optimization routines were applied afterwards to refine the structure using the free energy functional method.[27,28] To within atom displacements lower than 1 pm the final structure was found to belong to the space group $Fd3m$ setting 2 (relaxed lattice parameter $a_0 = 1.050$ nm) and the following asymmetric unit: Ce (16c), Zr (16d), O (48f, $x = 0.386224$), O (8a), and O (8b), see Figure 2a. The HREM image simulations calculated using EMS software from this model for 50/50 and 62/38 Ce/Zr molar fractions are in good agreement with the experimental ones reported in this paper and elsewhere.[29] In the case of a 62/38 molar fraction, 0.235 and 0.765 structural occupation factors for Ce and Zr, respectively, were considered for the 16d sites.[21] The FT obtained along the [110] zone axis (Figure 2c) shows the presence of the 1/2 {111} intermediate spots in addition to those due to the fluorite structure.

A comparison of the two HREM images in Figure 1 also reveals that after a SR-MO treatment some changes in the surface of the oxide particles take place. Low-magnification TEM views clearly reveal a transition from roundedlike crystallites to well-faceted oxide particles. A statistical analysis of the surface planes, performed on the basis of HREM images, indicates an increase of the extension of the {111} faces from 35% in the fresh oxide sample, up to about 60% in the SR-MO-treated oxide.

For a number of particles showing superstructure features, like that in Figure 1b, tomographic reconstructions were obtained from a series of HAADF images acquired between −70 and 70° every 2° and were processed using the FEI software Inspect 3D.[30] These tomograms reveal a shape very close to that of an octahedron (see Figure 3a). This observation is in good agreement with the observed increase of {111} facets in the SR-MO sample. Measurement of the angles between the exposed faces in a central slice through the nanocrystal (Figure 3b) confirms this fact, showing the values of 70 and 110° that are typical for octahedral morphology.

An important feature of the {111} facets in the SR-MO sample was revealed by high-resolution HAADF-STEM images (Figure 4a). The intensity profile of this HAADF image recorded along a line normal to the {111} fringes (Figure 4b) shows an alternating intensity sequence. To provide an interpretation to this contrast feature, we created a supercell, using Rhodius program,[24] projecting the DFT calculated structure along a general direction perpendicular to a (111) surface (Figure 5a). As seen in the projection, two different types of {111} plane exist in this cation-ordered phase, the difference between them being the molar ratio of Ce/Zr species: 4/1 in the Ce-rich one to 2/3 in the Zr-rich variant for a $Ce_{0.62}Zr_{0.38}O_2$ mixed oxide. So in accordance with the strong dependence of the intensity of HAADF contrasts on the average Z values in the atomic

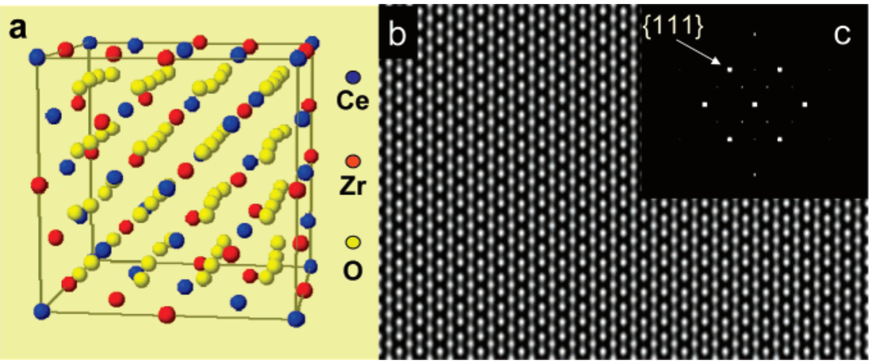

Figure 2. DFT calculated structure for a fully oxidized pyrochlore structure (a), HREM image simulations along [110] direction for a 12 nm thickness and Scherzer (43 nm) defocus (b), and its corresponding FT (c). The image simulations were carried out using the parameters for the JEOL 2010-FEG electron microscope.

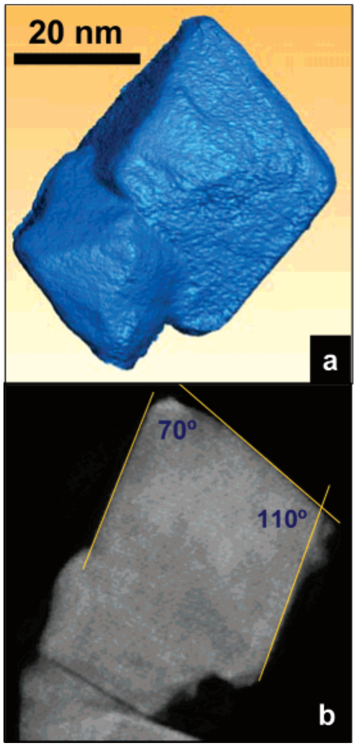

Figure 3. HAADF STEM tomogram (a) of a treated $Ce_{0.62}Zr_{0.38}O_2$ nanocrystal. A single central slice through the nanocrystal is shown in (b). The angles indicate the nanocrystal is octahedral in shape.

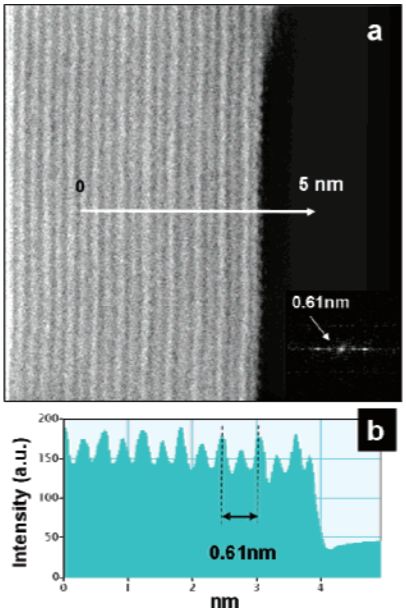

Figure 4. HAADF image (a) and its corresponding intensity profile along a direction perpendicular to the surface (b) of a SR-MO-treated $Ce_{0.62}Zr_{0.38}O_2$ nanocrystal. The fringe spacing, 0.61 nm, corresponds to the fluorite-like 1/2 {111} spots as seen in Figures 1b and 2c.

planes,[31] the lower intensity fringes in the HAADF image can be assigned to the Zr-rich {111} planes, whereas the higher intensity lines would correspond to Ce-rich planes.

Most importantly, a close inspection of Figure 4a and the intensity profile in Figure 4b reveals that for the uppermost surface plane, the {111} fringe corresponds to a low-intensity line (i.e., to a Zr-rich {111} plane). This is a general observation in all the analyzed HAADF images of the SR-MO sample.

To confirm the interpretation of the experimental HAADF data, image simulations[23] have been performed from several supercells like the one shown in Figures 5a. In this case, a constant thickness and a Zr-rich {111} -ended surface is considered. Both the calculated image (Figure 5b) and their intensity profile along [111] (Figure 5c) show all the contrast features observed in the experimental image of Figure 4.

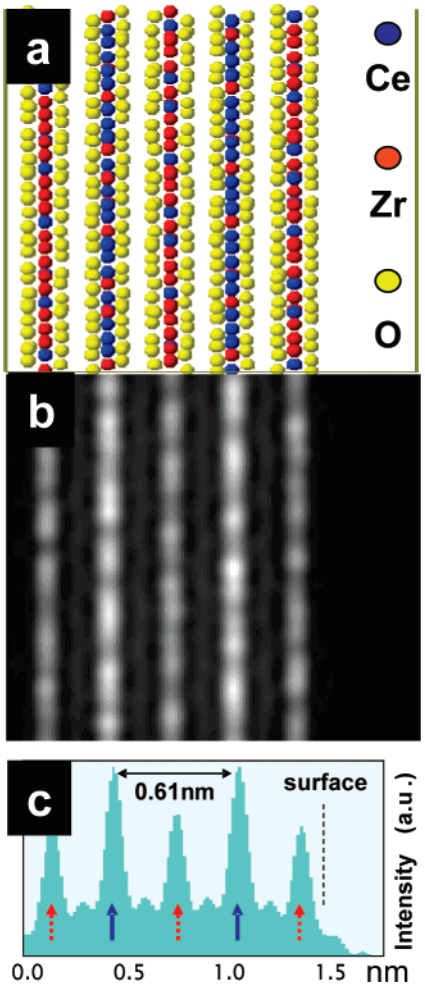

Figure 5. Super-cell (a) of the crystal structure projected through the [110] direction considering a 4.8 nm thickness crystal and a 7° tilting along [1−11]. The HAADF image simulation (b) and the intensity profile along a direction perpendicular to the surface (c) are also included. Solid blue arrows indicate Ce-rich planes, dashed red arrows indicate Zr-rich planes.

A qualitative interpretation of the presence of Zr-rich {111} surfaces in the SR-MO-treated sample could be as follows: during the high-temperature reduction treatment (SR) the pyrochlore structure is formed exposing the Zr-rich {111} surfaces. These are the ones containing a higher concentration of oxygen vacancies according to the bulk structure, and they are probably the most stable ones. These Zr-rich surfaces are oxidized during the MO step of the treatment, refilling the corresponding oxygen vacancies, but without the possibility at such low temperature to rearrange the cation sublattice. Surface energies DFT calculations are currently underway to confirm this interpretation and to investigate from the theoretical point of view the most stable morphology and surface chemical composition for this kind of materials.[32]

To summarize, the cation-ordering phenomena induced by the SR-MO treatment affects the surface of the fresh mixed oxide in two different ways: first, by increasing the percentage of exposed {111} type surfaces, and second, by imposing a specific type of {111} surface with a defined structure and chemical composition (Zr-rich). These changes could be key factors in understanding the distinct chemical behavior, for instance the capability for activating the hydrogen molecule dissociation,[16] observed in the SR-MO sample. We should also highlight the very interesting capabilities of HAADF-STEM imaging and tomography in the surface characterization of nanocrystalline mixed oxides and the DFT calculations for the modeling of complex structures.

Acknowledgment. We acknowledge the financial support from Spanish MEC/FEDER-EU (Project MAT2005-00333), and the *Junta de Andalucía* (Groups FQM-110 and FQM-334). EU I3 Project ESTEEM (Contract n° 026019 RII3) is also acknowledged. P.A.M. thanks the Isaac Newton Trust, the Royal Academy of Engineering, and the Leverhulme Trust for financial support. A.B.H. thanks the UE for the award of a Marie-Curie fellowship. J.A.P.O. thanks the Ministry of Education and Science of Spain for the awarding of a sabbatical stay at the Department of Chemistry in Cambridge, U.K.

Supporting Information Available: A HAADF electron tomographic reconstruction video clip and a Car−Parrinello molecular dynamics coordinates trajectory file animation. This material is available free of charge via the Internet at http://pubs.acs.org.

References and Notes

(1) Kaspar, J.; Fornasiero, P.; Hickey, N. *Catal. Today* **2003**, *77*, 419.

(2) Bernal, S.; Blanco, G.; Calvino, J. J.; Gatica, J. M.; Pérez-Omil, J. A.; Pintado, J. M. *Top. Catal.* **2004**, *28* (1−4), 31−45.

(3) Liotta, L. F.; Di Carlo, G.; Pantaleo, G.; Deganello, G. *Appl. Catal., B* **2007**, *70* (1−4), 314−322.

(4) Tibiletti, D.; Fonseca, A. A.; Burch, R.; Chen, Y.; Fisher, J. M.; Goguet, A.; Hardacre, C.; Hu, P.; Thompsett, D. *J. Phys. Chem. B* **2005**, *109* (47), 22553−22559.

(5) Serrano-Ruiz, J. C.; Luettich, J.; Sepulveda-Escribano, A.; Rodriguez-Reinoso, F. *J. Catal.* **2006**, *241* (1), 45−55.

(6) Trovarelli, A. *Catalysis by Ceria and Related Materials*; Imperial College Press: London, 2002.

(7) Di Monte, R.; Kaspar, J. *J. Mater. Chem.* **2005**, *15*, 633−648.

(8) Shah, P. R.; Kim, T.; Zhou, G.; Fornasiero, P.; Gorte, R. J. *Chem. Mater.* **2006**, *18* (22), 5363−5369.

(9) Alessandri, I.; Bañares, M. A.; Depero, L. E.; Ferroni, M.; Fornasiero, P.; Gennari, F. C.; Hickey, N.; Martinez-Huerta, M. V.; Montini, T. *Top. Catal.* **2006**, *V41* (1), 35−42.

(10) Montini, T.; Hickey, N.; Fornasiero, P.; Graziani, M.; Bañares, M. A.; Martínez-Huerta, M. V.; Alessandri, I.; Depero, L. E. *Chem. Mater.* **2005**, *17*, 1157−1166.

(11) Montini, T.; Bañares, M. A.; Hickey, N.; Di Monte, R.; Fornasiero, P.; Kaspar, J.; Graziani, M. *Phys. Chem. Chem. Phys.* **2004**, *6*, 1−3.

(12) Fornasiero, P.; Montini, T.; Graziani, M.; Kaspar, J.; Hungria, A. B.; Martinez-Arias, A.; Conesa, J. C. *Phys. Chem. Chem. Phys.* **2002**, *4* (1), 149−159.

(13) Baker, R. T.; Bernal, S.; Blanco, G.; Cordon, A. M.; Pintado, J. M.; Rodriguez-Izquierdo, J. M.; Fally, F.; Perrichon, V. *Chem. Commun.* **1999**, *2*, 149−150.

(14) Izu, N.; Omata, T.; Otsuka-Yao-Matsuo, S. *J. Alloys Compd.* **1998**, *270* (1−2), 107−114.

(15) Otsuka-Yao-Matsuo, S.; Omata, T.; Izu, N.; Kishimoto, H. *J. Solid State Chem.* **1998**, *138* (1), 47−54.

(16) Yeste, M. P.; Hernandez, J. C.; Bernal, S.; Blanco, G.; Calvino, J. J.; Perez-Omil, J. A.; Pintado, J. M. *Chem. Mater.* **2006**, *18*, 2750−2757.

(17) Perez-Omil, J. A.; Bernal, S.; Calvino, J. J.; Hernandez, J. C.; Mira, C.; Rodriguez-Luque, M. P.; Erni, R.; Browning, N. D. *Chem. Mater.* **2005**, *17* (17), 4282−4285.

(18) Suda, A.; Ukyo, Y.; Yamamura, K.; Sobukawa, H.; Sasaki, T.; Nagai, Y.; Tanabe, T.; Sugiura, M. *J. Ceram. Soc. Jpn.* **2004**, *112*, 586−589.

(19) Sasaki, T.; Ukyo, Y.; Kuroda, K.; Arai, S.; Saka, H. *J. Electron. Microsc.* **2003**, *52* (3), 309−312.

(20) Thomson, J. B.; Armstrong, A. R.; Bruce, P. G. *J. Am. Chem. Soc.* **1996**, *118* (45), 11129−11133.

(21) Withers, R. L.; Thompson, J. G.; Barlow, P. J.; Barry, J. C. *Aust. J. Chem.* **1992**, *45* (9), 1375−1395.

(22) Stadelmann, P. A. *Ultramicroscopy* **1987**, *21* (2), 131−145.

(23) Kirkland, E. J. *Advanced Computing in Electron Microscopy*; Plenum Press: New York, 1998.

(24) Bernal, S.; Botana, F. J.; Calvino, J. J.; Lopez-Cartes, C.; Perez-Omil, J. A.; Rodriguez-Izquierdo, J. M. *Ultramicroscopy* **1998**, *72* (3−4), 135−164.

(25) Midgley, P. A.; Weyland, M.; Thomas, J. M.; Johnson, B. F. G. *Chem. Commun.* **2001**, *10*, 907−908.

(26) Car, R.; Parrinello, M. *Phys. Rev. Lett.* **1985**, *55* (22), 2471.

(27) Hutter, J.; Alavi, A.; Deutch, T.; Bernasconi, M.; Goedecker, S.; Marx, D.; Tuckerman, M.; Parrinelo, M. http://www.cpmd.org (accessed 2006), CPMD, version 3.11, IBM Corp and MPI Stuttgart.

(28) Alavi, A.; Kohanoff, J.; Parrinello, M.; Frenkel, D. *Phys. Rev. Lett.* **1994**, *73* (19), 2599.

(29) Baker, R. T.; Bernal, S.; López-Cartes, C.; Pérez-Omil, J. A.; Montardi, Y. *Inst. Phys. Conf. Ser.* **1999**, *161* (Section 10), 521.

(30) Midgley, P. A.; Weyland, M. *Ultramicroscopy* **2003**, *96* (3−4), 413−431.

(31) Browning, N. D.; James, E. M.; Kishida, K.; Arslan, I.; Buban, J. P.; Zaborac, J. A.; Pennycook, S. J.; Xin, Y.; Duscher, G. *Rev. Adv. Mater. Sci.* **2000**, *1* (1), 1−26.

(32) Perez-Omil, J. A.; Alavi, A. Unpublished work.